RSC Advances

PAPER

View Article Online
View Journal | View Issue

Cite this: *RSC Adv.*, 2025, **15**, 40730

Synthesis and solvatochromism of a NIR II emissive amphiphilic aza-BODIPY dye and its application as a colorimetric and fluorometric probe in sequential detection of Cu^{2+} and PO_4^{3-}

Mengqi Liu,[a] Xuefeng Kuang,[a] Junjun Su,[a] Hongfei Pan,[ab] Mengyu Hao[a] and Zhijian Chen *[a]

The amphiphilic aza-BODIPY **1** bearing two *N*,*N*-dialkyl-amino groups at the *para*-positions of the 1,7-phenyl and two amino groups modified by a pair of hydrophilic chains at the *para*-positions at the 3,5-phenyl of the boron-azadipyrromethene core was synthesized and characterized. UV/Vis/NIR spectroscopic measurements indicated that the S_0–S_1 absorption band **1** reached up to 900 nm while its emission band reached up to 1200 nm. The solvatochromic properties of **1** was investigated by absorption and fluorescence spectroscopy and further analysed by the Lippert–Mataga equation. The results suggested a strong intramolecular charge transfer (ICT) effect of dye **1** stemming from the electron-donating amino groups, which was further confirmed by DFT calculation studies. Such ICT could be disrupted upon addition of Cu^{2+} owing to the metal–ligand interaction between Cu^{2+} and the amino moieties, leading to a hypsochromic shift of the absorption band concomitant with a significant decrease in the fluorescence intensity of **1**. Moreover, the spectroscopic properties of **1** were recovered upon subsequent addition of PO_4^{3-} in [**1** + Cu^{2+}] solution. Based on these observations, the dye **1** was applied successfully as a NIR colorimetric and fluorometric "turn-off" probe for selective detection of Cu^{2+} (LOD = 2.1 μM). Subsequent fluorometric "turn-on" detection of PO_4^{3-} by [**1** + Cu^{2+}] (LOD = 3.0 μM) was accomplished in further studies.

Received 8th September 2025
Accepted 18th October 2025

DOI: 10.1039/d5ra06752a

rsc.li/rsc-advances

Introduction

In recent years, functional dyes with near-infrared absorption and emission (NIR dyes)[1] have received widespread attention owing to their attractive potential in a variety of applications such as agents for phototherapy,[2] organic photovoltaics,[3] as well as fluorescence probes.[4] For the latter, the common probes operated within the ultraviolet/visible (UV/Vis) range could be limited by the background fluorescence interference, light scattering, or photodamage of the samples.[5] In contrast, the fluorescent probes functioned in the NIR-I (650–950 nm) and NIR-II (1000–1700 nm) windows[6] exhibited unique advantages including reduced susceptibility to background interference, high signal-to-noise ratio, less scattering and deeper penetration depth, and negligible impairment for biological samples.[7] Accordingly, NIR fluorescent sensing probes based on cyanine,[8] perylene diimide,[9] rhodamine,[10] BODIPYs,[11] *etc.* have been developed and applied for the detection of various metal ions as well as small molecules.[12]

As an important class of NIR chromophore, BF_2-azadipyrromethenes (aza-BODIPYs)[13] exhibited intensive absorption and emission bands, high fluorescence quantum yields, as well as excellent stability. Moreover, the π-conjugate structure of the aza-BODIPY is facile to be chemically modified by introducing heavy atoms,[14] incorporating strong electron-donating groups to form a push–pull electronic structure,[15] and ring-fusing to form expanded conjugate structures of the aza-BODIPY dyes.[16] Based on these methods, the optical properties of aza-BODIPYs can be adjusted and their absorption and emission bands can be effectively shifted toward longer wavelengths in comparison with the parent tetraphenyl-substituted aza-BODIPY (λ_{abs} = 650 nm, λ_{em} = 673 nm).[17] For examples, the aza-BODIPY dyes bearing electron-donating triphenylamine[18] and julolidine[19] units were synthesized, which exhibited emission maxima at 892 and 1060 nm, respectively. Hao, Jiao, and coworkers[20] developed strategies for the synthesis of thieno-, and naphtho-fused aza-BODIPY dyes with their emission peaks at 816 nm and 705–972 nm, respectively.

While tremendous progresses were made in the synthesis of NIR absorbing aza-BODIPYs, fluorescent probes based on this class of dyes were developed for detecting various analytes,[21] including metal ions (Cu^{2+}, Hg^{+}),[22] anions (NH_4^+, F^-, NO_2^-),[23]

[a]*School of Chemical Engineering and Technology, Tianjin University, Tianjin 300072, China. E-mail: zjchen@tju.edu.cn*
[b]*Zhejiang Institute of Tianjin University, Ningbo, 315201, PR China*

and small molecules (H_2O_2, H_2S, NO).[24] Noteworthy that in recent years some sequential ion-responsive systems that were capable of detecting two different analytes have been reported. For examples, Kim *et al.*[25] developed a colorimetric probe for sequential detection of Cu^{2+} and CN^-. In another work, Ren *et al.*[26] synthesized a self-assembling tetraphenylethylene derivative for sequential detection of Fe^{3+} and F^-. Nevertheless, the sequential ion-responsive properties and detection of different analytes have not been reported yet for aza-BODIPY dyes, to the best of our knowledge.

In the current work, we reported the synthesis, photophysical properties, and sequential ion-responsive characteristics of an amphiphilic aza-BODIPY dye **1**. By introducing four electron-donating *N*,*N*-disubstituted amino groups at the *para*-positions of 1,3,5,7-phenyl substituents at the aza-BODIPY core, in polar solvent the dye **1** exhibited an emission band that reached the NIR-II window. In addition, the dye **1** bear two hydrophobic *N*,*N*-dodecyl groups at the 1,7-phenyl positions and four hydrophilic pendant containing oligo-ethylene glycol (OEG) chains. Such an amphiphilic feature of dye **1** offered good solubilities in both polar and nonpolar solvents, allowing the investigation of the solvatochromic properties of this dye in a wide range of solvents. Furthermore, the potential application of dye **1** as a colorimetric and fluorescent probe for the continuous detection of Cu^{2+} and PO_4^{3-} was also explored, which are known to be common environmental pollutants leading to health risks[22a–c] and deterioration of water quality.[27]

Results and discussion

Synthesis and spectroscopic properties of dye 1

The synthetic route of the amphiphilic aza-BODIPY dye **1** was illustrated in Scheme 1. The chalcone derivative **4** was formed by the aldol condensation between the compounds **5** and **6**. The subsequent Michael addition between **4** and nitromethane was performed by using a 5-fold excess of nitromethane in ethanol at 80 °C for 12 h, affording intermediate **3**. Further condensation of **3** and ammonium acetate (15 equiv.) in refluxing *n*-butanol (110 °C, 12 h) gave the intermediate azadipyrromethene, which was subsequently converted into aza-BODIPY **2** by chelation of $BF_3 \cdot Et_2O$ in dried CH_2Cl_2 under N_2 atmosphere. In the last step, the amphiphilic aza-BODIPY dye **1** was obtained by attaching four oligo-ethylene glycol (OEG) hydrophilic pendants to the aza-BODIPY **2** with CuI-catalysed click reaction. The target dye **1** was characterized by ^1H NMR, ^{13}C NMR and MALDI-TOF mass spectroscopy (for details, see SI).

The UV/Vis/NIR absorption spectrum (black) of the amphiphilic dye **1** in $CHCl_3$ (1.0×10^{-6} M) was shown in Fig. 1a. An intensive band in NIR with a absorption maximum at 806 nm ($\varepsilon = 9.5 \times 10^4$ M^{-1} cm^{-1}) was observed, which could be assigned to the S_0–S_1 transition of aza-BODIPY **1**.[28] This absorption maximum of **1** manifested a substantial bathochromic shift of 156 nm with respect to that of the parent tetraphenyl-substituted aza-BODIPY ($\lambda_{abs} = 650$ nm, $\lambda_{em} = 673$ nm),[17] which could be attributed to the introduction of the four *para*-dimethylaniline electron-donating into the molecular structure of dye **1**. In addition, the lower absorption band of dye **1** between 600 nm and 700 nm could be assigned to the S_0–S_2 transition of this dye.

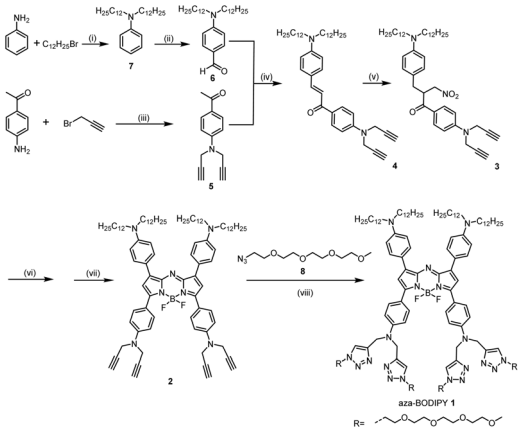

Scheme 1 Synthesis of aza-BODIPY **1**. Reagents and conditions: (i) K_2CO_3, DMF, r.t., 80 °C, 24 h; (ii) $POCl_3$, DMF, r.t.; 79%; (iii) K_2CO_3, DMF, r.t., 24 h; 43%; (iv) *t*-BuOK, ethanol, r.t., 12 h; 41%; (v) *t*-BuOK, CH_3NO_2, ethanol, r.t., 80 °C, 24 h; 56%; (vi) CH_3COONH_4, *n*-butanol, 110 °C, 12 h; (vii) $BF_3 \cdot Et_2O$, dry CH_2Cl_2, DIEA, r.t., 12 h; 21%; (viii) CuI, DIEA, CH_2Cl_2, CH_3CN, 60 °C, 8 h; 82%.

In Fig. 1a, the fluorescence spectrum (red) of aza-BODIPY **1** demonstrated a mirror relationship with its absorption spectrum, featuring a narrow-emission band with $\lambda_{em} = 863$ nm and a Stokes shift of 57 nm. Meanwhile, a fluorescence quantum yield $\Phi_{fl} = 0.16$ was determined for **1**. Moreover, the fluorescence lifetime of **1** was measured by time-resolved fluorescence spectroscopy (Fig. 1b). An average fluorescence lifetime $\langle\tau\rangle = 4.00$ ns was obtained for dye **1** by fitting the decay curve with a biexponential model ($\tau_1 = 1.39$ ns, 92.66% and $\tau_2 = 37.00$ ns, 7.34%).

Solvatochromic properties of dye 1

To shed more light on the large bathochromic shift of the S_0–S_1 absorption band of **1** with respect to that of the tetraphenyl-substituted the aza-BODIPY dye, the solvatochromic properties of dye **1** were investigated by absorption and emission spectroscopy in organic solvents of various polarity (Fig. 2 and Table 1).

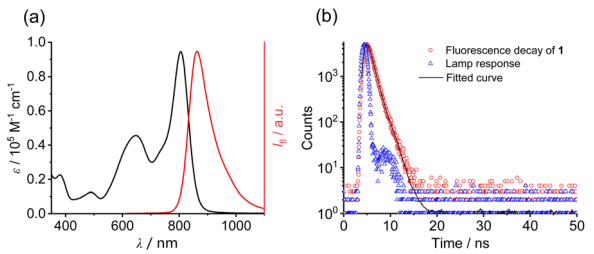

Fig. 1 (a) UV/Vis/NIR absorption and fluorescence spectra of dye **1** in $CHCl_3$ ([**1**] = 1.0×10^{-6} M, $\lambda_{ex} = 600$ nm); (b) fluorescence decay spectra of dye **1** in $CHCl_3$ ([**1**] = 1.0×10^{-6} M, $\lambda_{ex} = 600$ nm, $\lambda_{em} = 820$ nm).

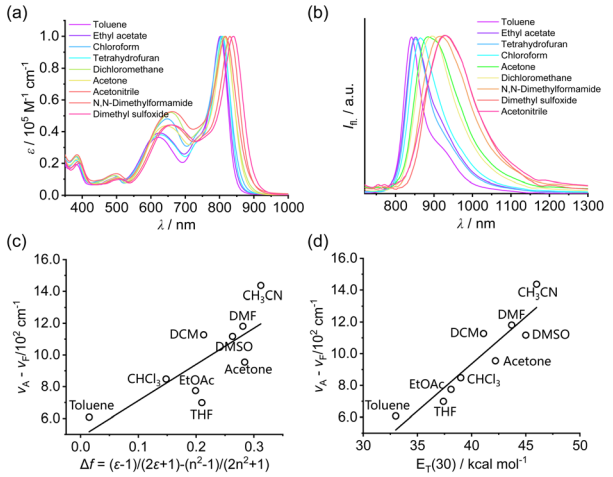

Fig. 2 UV/Vis/NIR absorption spectra (a) and fluorescence spectra (b) of dye **1** in different organic solvents; (c) Lippert equation of dye **1** in different organic solvents; (d) the relationship between the Stokes shift ($\nu_A - \nu_F$) of dye **1** and the empirical polarity parameter $E_T(30)$ of different organic solvents. ([**1**] = 1.0 × 10^{-6} M, λ_{ex} = 700 nm).

Table 1 Spectral properties of dye **1** in different solvents, including chloroform ($CHCl_3$), *N*,*N*-dimethylformamide (DMF), acetonitrile (CH_3CN), tetrahydrofuran (THF), dimethyl sulfoxide (DMSO), dichloromethane (CH_2Cl_2), ethyl acetate (EtOAc), toluene, acetone

Solvent	ε^a	n^b	Δf^c	$\lambda_A{}^d$/nm	$\lambda_F{}^e$/nm	$(\nu_A - \nu_F)^f$/cm^{-1}
Toluene	2.4	1.496	0.015	801	842	608
EtOAc	6.0	1.372	0.199	801	854	775
$CHCl_3$	4.8	1.447	0.148	805	864	848
THF	7.6	1.407	0.210	805	853	699
CH_2Cl_2	8.5	1.424	0.213	813	895	1127
Acetone	20.7	1.359	0.284	816	885	955
CH_3CN	37.5	1.344	0.312	818	927	1437
DMF	36.7	1.431	0.281	829	919	1181
DMSO	46.7	1.478	0.263	840	927	1117

[a] Permittivity of solvent. [b] Refractive index of solvent. [c] $\Delta f = [(\varepsilon - 1)/(2\varepsilon + 1)] - [(n^2 - 1)/(2n^2 + 1)]$. [d] Absorption maxima. [e] Emission maxima. [f] Stokes shift.

As shown in Fig. 2a, the absorption maxima of dye **1** in different solvents were located between 801–840 nm, depending on the solvent polarity. In contrast to the absorption spectra, much larger shift of the emission maxima was observed in the fluorescence spectra of dye **1** (Fig. 2b) in different solvents. With increase in solvent polarity, the emission maxima exhibited a considerable red-shift from 842 nm (toluene) to 927 nm (DMSO), indicating a positive solvatochromic effect[29] of dye **1**.

Based on the spectroscopic data summarized in Table 1, the solvatochromic properties of dye **1** were further analysed by Lippert–Mataga eqn (1),[30]

$$hc(\nu_A - \nu_F) = 2\Delta f \frac{(\mu_E - \mu_G)^2}{a^3} + C \quad (1)$$

where ν_A and ν_F were the absorption and emission maxima in wave numbers dye **1** (cm^{-1}), μ_G and μ_E were the dipole moments

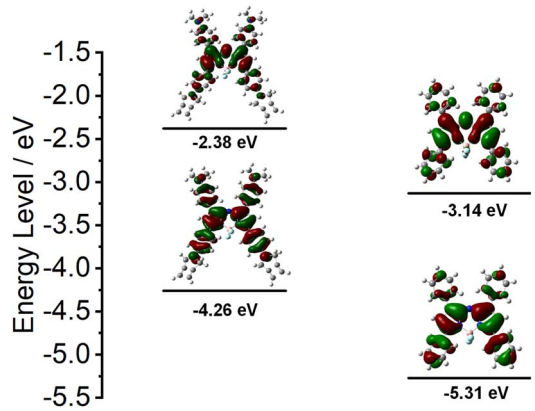

Fig. 3 Distributions of HOMO and LUMO and energy levels of a model compound for **1** (left, the hydrophobic and hydrophilic chains in **1** were replaced by methyl groups) and tetraphenyl-substituted aza-BODIPY. DFT calculations were carried out on the Gaussian 09W software platform, using B3LYP as the method and 6-311G(d) as the base group.

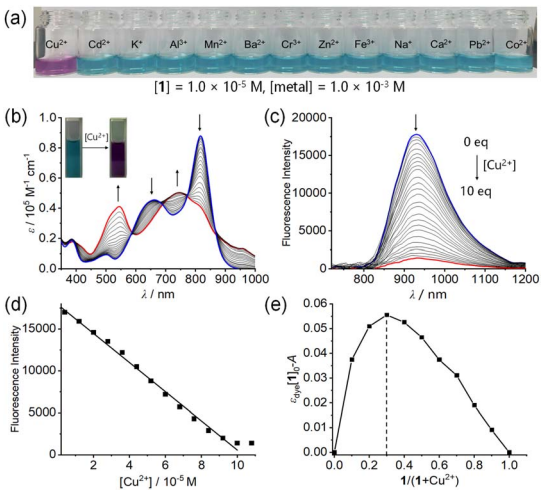

Fig. 4 (a) The colours of the solutions after adding different metal ions. ([**1**] = 1.0 × 10^{-5} M, [metal] = 1.0 × 10^{-3} M); (b) UV/Vis absorption spectra (Inset: Colour change of the solution after adding Cu^{2+}); (c) fluorescence spectra of dye **1** in CH_3CN/H_2O (v/v, 10 : 1); (d) plot of the fluorescence intensity of the system with different concentrations of Cu^{2+}; (e) Job's plot of dye **1** and Cu^{2+} in CH_3CN. (The absorbances (*A*) of the solutions at 818 nm were used for analysis.)

of the ground state and excited state respectively, *h* was the Planck's constant, *c* was the velocity of light, *a* was the radius of the cavity where the fluorophore was located (Onsager radius), and Δf was the solvent parameter, which was defined as $[(\varepsilon - 1)/(2\varepsilon + 1)] - [(n^2 - 1)/(2n^2 + 1)]$.

As shown in Fig. 2c, we observed an approximate linear relationship between the Stokes shifts ($\nu_A - \nu_F$) of dye **1** and the solvent parameters (Δf). Based on the slope $(2/hc)[(\mu_E - \mu_G)^2/a^3]$[31] obtained by linear fitting and a cavity radius $a = 0.51$ nm of the chromophore, which was estimated according to the molecular modelling, the change of dipole moment between the excited state and the ground state ($\Delta\mu_{eg}$) of dye **1** was calculated to be 1.74 D, indicating that the dipole moment of

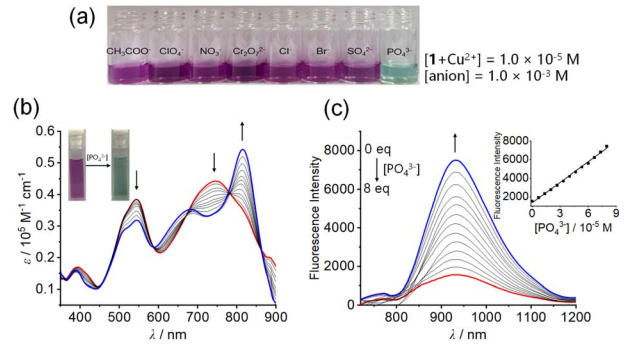

Fig. 5 (a) The colours of the solutions after adding different anions. ([**1** + Cu^{2+}] = 1.0 × 10^{-5} M, [anion] = 1.0 × 10^{-3} M); (b) UV/Vis absorption spectra (Inset: Colour change of the solution after adding PO_4^{3-}); (c) fluorescence spectra of this system in CH_3CN/H_2O (v/v, 50 : 9) (Inset: Plot of the fluorescence intensity of the system with different concentrations of PO_4^{3-}).

Table 2 Comparisons between dye **1** and literature-reported probes **A**–**G** (mostly BODIPY/aza-BODIPY-based, see Fig. S33 for chemical structures) for detection of Cu^{2+} or PO_4^{3-} or for sequential ion-detection

Probe	λ_{abs} [a]	λ_{em} [b]	Φ_{fl} [c]	$LOD_{Cu^{2+}}$	LOD_{anion}
1	818	927	0.16	2.1 μM	3.0 μM
A[d]	450	N.A.	N.A.	0.9 μM	(CN^-)
B[e]	N.A.	420	N.A.	N.A.	19.69 mM
C[f]	503	580	0.34	6 μM	N.A.
D[g]	686	720	N.A.	N.A.	N.A.
E[h]	680	717	N.A.	0.2 μM	N.A.
F[i]	690	725	N.A.	3.75 ppb	N.A.
G[j]	784	840	0.29	1.38 μM	N.A.

[a] Absorption Maximum. [b] Emission maximum. [c] Fluorescence quantum yield. [d] Ref. 25. [e] Ref. 27. [f] Ref. 41. [g] Ref. 11. [h] Ref. 22*a*. [i] Ref. 22*b*. [j] Ref. 15*b*.

the excited state of the dye was greater than that of the ground state. This result ($\mu_E > \mu_G$) could be explained by the formation of intramolecular charge transfer (ICT) state upon excitation of dye **1**.[32] Such an ICT state could be stabilized upon increase in the solvent polarity. Accordingly, a positive solvatochromic effect was displayed by dye **1**.

In addition, while the empirical solvent polarity parameter $E_T(30)$[33] was used to study the relationship between the Stokes shifts of dye **1** and solution polarity (Fig. 2d), a correlation coefficient $r = 0.93$ was obtained, indicating that the correlation was significantly improved as compared with that using Δf.

In order to further elucidate the ICT characteristics of dye **1**, density functional theory (DFT) calculations were performed for a model compound of dye **1** (in which the side chains were replaced by methyl groups) as well as the tetraphenyl-substituted aza-BODIPY (Fig. 3). The results suggested that the HOMOs of **1** were delocalized over the entire molecular framework. In contrast, the LUMOs of **1** were mainly located on the aza-BODIPY core with an obvious contribution of the *meso*-N atom. Such separation between HOMO and LUMO implied that ICT might take place between the electron-donating amino groups and the electron-accepting aza-BODIPY core upon excitation of dye **1**. In contrast, tetraphenyl-substituted aza-BODIPY displayed a less extensive HOMO than the model compound. In addition, the calculation pointed to a smaller band gap of dye **1** than that of tetraphenyl-substituted aza-BODIPY, which was in agreement with the results of spectroscopic studies.

Colorimetric and fluorometric "turn-off" probe for Cu^{2+}

Since it has been reported that the bis(1,2,3-triazole) amino group was effective ligand for metal ions,[34] the application potential of dye **1** as sensor for metal ion detection was investigated. Accordingly, solutions of various metal ions (1.0 × 10^{-3} M) in water (10 equiv.) were added to dye **1** solutions (1.0 × 10^{-5} M) in CH_3CN. The latter was not only a good solvent for dye **1** but also miscible with water and used widely in ion-detection studies.[11,15b,35] While the colour of the dye solution changed remarkably from blue to purple upon adding of Cu^{2+}, no colour changes were observed by naked eyes upon adding of the other metal ions, including Cd^{2+}, K^+, Al^{3+}, Mn^{2+}, Ba^{2+}, Cr^{3+}, Zn^{2+}, Fe^{3+}, Na^+, Ca^{2+}, Pb^{2+}, Co^{2+} (Fig. 4a), implying that dye **1** could be used for selective detection of Cu^{2+}. This was further confirmed by the absorption and fluorescence spectroscopic measurements (Fig. S23). In the presence of Cu^{2+}, significant spectral changes were observed in the absorption and fluorescence spectra of dye **1**. In contrast, negligible spectral responses of the dye **1** solutions were detected for other ions. Thus, the aza-BODIPY **1** could serve as a highly selective colorimetric and NIR fluorometric "turn-off" probe[36] for Cu^{2+}.

To quantitatively elucidate the binding between dye **1** and Cu^{2+}, UV/Vis and fluorescence spectroscopic titration studies were performed. Upon gradual addition of up to 10 equiv. of Cu^{2+}, gradual lowering of the S_0–S_1 (around 818 nm) and S_0–S_2 band (around 659 nm) was observed (Fig. 4b). The absorption maximum was hypsochromically shifted from 818 nm to 745 nm, indicating that the ICT effect in dye **1** could be disrupted by the metal–ligand interactions between Cu^{2+} and the bis (1,2,3-triazole) amino groups. Meanwhile, new absorption bands gradually raised at around 745 nm and 544 nm. Such absorption spectra changes were in agreement with the colour change of the dye solution upon adding the Cu^{2+}. Moreover, decrease in the fluorescence intensity at around 955 nm was observed upon the addition of Cu^{2+} (Fig. 4c). The plot of fluorescence intensity *versus* the concentration of Cu^{2+} exhibited a good linear relationship ($R^2 = 0.9954$), demonstrating that dye **1** was capable of detecting Cu^{2+} quantitatively. The Stern–Volmer plot[37] based on the fluorescence spectra (Fig. S24) of dye **1** gave a quenching constant $K_{SV} = 3.7 \times 10^4$ M^{-1} by linear data fitting. Based on the change of fluorescence spectra at 929 nm, the limit of detection (LOD)[38] for Cu^{2+} was determined to be 2.1 μM (Fig. S25).

To verify the binding stoichiometry between the dye **1** and Cu^{2+}, Job's plot analysis was performed for the absorbance variations at 818 nm (Fig. 4e) and the result unambiguously pointed to a 1 : 2 binding stoichiometry of **1** and Cu^{2+}.Thus, each of the bis(1,2,3-triazole) amino moieties in dye **1** was

bound to one Cu^{2+} and a bimetallic complex of **1** was formed. This was further confirmed by the mass spectroscopic (MALDI-TOF) measurement of the complex (Fig. S26), which indicated the formation of species **1** + 2Cu^{2+} (*m*/*z* 610.5, calculated: 610.5) and **1** + Cu^{2+} (*m*/*z* 1189.9, calculated: 1189.3). The binding constant of dye **1** and Cu^{2+} could be estimated by using eqn (2),[39]

$$\frac{[H]_0[G]_0^{\,2}}{\Delta A} = \frac{1}{\Delta\varepsilon_a K} + \frac{[G]_0([G]_0 + 4[H]_0)}{\Delta\varepsilon_a} \quad (2)$$

where $[H]_0$ and $[G]_0$ were the initial concentrations of **1** (host) and Cu^{2+} (guest), respectively, and ΔA and $\Delta\varepsilon_a$ represented the changes of absorbance and molar absorption coefficient after complexation, respectively. By linear least-squares fitting with eqn (2), an overall binding constant $K = 2.0 \times 10^9\ M^{-2}$ was obtained (Fig. S27).

In addition, competitive binding test was conducted to evaluate the Cu^{2+} selectivity of **1** by introducing 10 equiv. excess of competing cations into the **1** + Cu^{2+} complex (1 : 2 stoichiometry), including Cd^{2+}, K^+, Al^{3+}, *etc.* The fluorescence spectra of **1** (Fig. S28) indicated that, the fluorescence intensity of the solutions remained unchanged before and after the addition of other metal ions, indicating that Cu^{2+} in the complex could not be replaced by other metal ions and had a good anti-interference capability for the detection of Cu^{2+}.

Fluorometric "turn-off-on" probe for sequential detection of PO_4^{3-}

Since the dye **1** was capable of chelating with Cu^{2+}, it was attractive to further investigate the response properties and potential of the [**1** + Cu^{2+}] system in sequential detection of anions.[25] Accordingly, a variety of common anions in water including PO_4^{3-}, ClO_4^-, Cl^-, Br^-, NO_3^-, $Cr_2O_7^{2-}$, SO_4^{2-}, CH_3COO^- were introduced into solution of [**1** + Cu^{2+}]. Upon addition of PO_4^{3-}, the colour of the dye **1** solution was changed to be blue-green. Meanwhile, no colour changes were observed for the solution upon addition of the other anions (Fig. 5a), suggesting a selective response of [**1** + Cu^{2+}] to PO_4^{3-}, which was corroborated by monitoring the absorption and fluorescence spectral changes in the presence of various of anions (Fig. S29).

As shown in Fig. 5b and c, the absorption bands of dye **1** were increased with the increasing concentration of PO_4^{3-} while the fluorescence intensity of **1** was increased drastically. This result indicated that PO_4^{3-} might have a stronger binding capability to Cu^{2+} than that of **1**, leading to the disassembly of [**1** + Cu^{2+}] species and the recovery of fluorescence of **1**. In addition, the fluorescence intensity of the system exhibited a good linear relationship with the concentration of PO_4^{3-} (R^2 = 0.9984, Fig. 5c inset). Moreover, the LOD for the detection of PO_4^{3-} was determined to be 3.0 μM (Fig. S30). To further verify the specificity of PO_4^{3-} detection, competition experiments were conducted (Fig. S31) and the results indicated that there was no significant change in the fluorescence intensity of the system in the presence of other anions, demonstrating that this "turn-off-on"[40] probing system for PO_4^{3-} detection was effective in complex ionic environments.

The reversibility of the probing system after adding Cu^{2+} and PO_4^{3-} was evaluated. Upon further adding Cu^{2+} and PO_4^{3-}, the absorption bands of dye **1** and [**1** + Cu^{2+}] was further recovered (Fig. S32), indicating the reversible ion-responsive behaviour of dye **1**. In addition, parameters of dye **1** and representative probes **A–G** for detection of Cu^{2+} or PO_4^{3-} or for sequential ion-detection (mostly BODIPY/aza-BODIPY-based, see Fig. S33 for chemical structures) were listed in Table 2. These data indicated that dye **1** exhibited moderate LODs of Cu^{2+} and PO_4^{3-} with the other probes. Meanwhile, aza-BODIPY **1** displayed the longest wavelength of absorption (818 nm) and emission maximum (927 nm), underscoring its better applicability as ion probes for biological systems.

Conclusions

In summary, a new amphiphilic NIR aza-BODIPY dye **1** bearing four hydrophobic alkyl chains and four hydrophilic oligo-ethylene glycol chains was synthesized and characterized. By introducing four *N*,*N*-double substituted amino groups as electron donating groups into dye **1**, it exhibited attractive NIR spectroscopic properties with absorption wavelength up to 950 nm and emission wavelength up to 1200 nm. A positive solvatochromism was observed for dye **1**. Further analysis of the solvent-dependent spectroscopic properties by Lippert–Mataga equation and DFT calculation studies indicated that the large bathochromic spectral shift of **1** with respect to the parent tetraphenyl-substituted aza-BODIPY could be ascribed to the strong ICT effect stemming from the electron-donating amino groups. Further observations of solution colour changes by naked eye and spectroscopic measurements implied that the ICT process in dye **1** could be disrupted upon addition of Cu^{2+} and recovered upon subsequent addition of PO_4^{3-}. Accordingly, the dye **1** was applied as a NIR colorimetric and fluorometric "turn-off" probe for selective detection of Cu^{2+} with a LOD of 2.1 μM. In addition, the complex [**1** + Cu^{2+}] was demonstrated to be a fluorometric "turn-on" probe for the detection of PO_4^{3-} with a LOD of 3.0 μM.

Experimental section

All the reagents and solvents in the synthesis were obtained from commercial suppliers and were not purified. All solvents used for spectral measurements were chromatographically pure and required no further purification. Details of the synthesis and characterization of intermediates **2–8** were provided in SI.

General methods

^1H and ^{13}C NMR spectra were recorded on Bruker AVANCE III HD 400 MHz or JEOL JNM ECZ600R spectrometer at room temperature. Chemical shifts (δ) were given in ppm relative to $CDCl_3$ (7.26 ppm for ^1H and 77 ppm for ^{13}C) to internal TMS. Mass spectra was measured by Autoflex III matrix-assisted laser desorption ionization time-of-flight (MALDI-TOF) mass spectrometry with α-cyano-4-hydroxycinnamic acid as the matrix. UV-Vis-NIR absorption spectroscopic measurements were

performed on UV-3600 (Shimadzu) or Carry 300 (Agilent) spectrophotometer. All measurements were made at 25 °C, using 10 × 10 mm cuvettes. Molar absorption coefficient ε was calculated according to Lambert–Beer's law.

Fluorescence spectroscopic measurement

The fluorescence spectra, fluorescence quantum yield of **1**, and fluorescence lifetimes were measured by a FLS 1000 spectrofluorometer (Edinburgh). All the fluorescence spectra were corrected. The fluorescence quantum yield of dye **1** was measured by using a built-in integrating sphere in the spectrofluorometer. The fluorescence lifetime measurements were performed with a time-correlated single photon counting setup consisting of a pulsed light emitting diode laser excitation source (λ_{ex} = 635 nm). The instrument response was collected by scattering the excited light of a dilute, aqueous suspension of colloidal silica (Ludox). The lifetime decay curves were analysed using the software supplied with the instrument. The quality of the data fitting was evaluated by analysis of χ^2 (0.9–1.1) as well as by inspection of residuals and the autocorrelation function.

Synthesis of aza-BODIPY 1

Compound **2** (0.138 g, 0.1 mmol) was dissolved in the mixed solvent of CH_2Cl_2/CH_3CN (40 mL, 1/1, v/v), and then CuI (0.019 g, 0.1 mmol), DIEA (18 drops), and compound **8** (0.198 g, 0.8 mmol) were added. The resultant reaction mixture was stirred for 8 h at 60 °C. After the reaction was completed (monitored by TLC), the solvent was rotary-evaporated. The oily residue was dissolved in CH_2Cl_2 and washed with water (3 × 50 mL). The combined organic layers were dried over $MgSO_4$ and concentrated. Further purification by column chromatography (silica gel, 300–400 mesh) using MeOH/CH_2Cl_2 (1/15, v/v) as the eluent gave the aza-BODIPY dye **1** as a blue-black solid (0.175 g, 82%). ^{1}H NMR (600 MHz, chloroform-*d*): δ = 8.03 (d, J = 8.4 Hz, 8H), 7.67 (s, 4H), 6.93 (d, J = 7.7 Hz, 4H), 6.81 (s, 2H), 6.67 (d, J = 8.6 Hz, 4H), 4.80 (s, 8H), 4.50 (s, 8H), 3.83 (d, J = 4.9 Hz, 8H), 3.54–3.30 (m, 68H), 1.63 (d, J = 7.3 Hz, 8H), 1.33 (d, J = 27.9 Hz, 72H), 0.87 (t, J = 7.0 Hz, 12H). ^{13}C NMR (101 MHz, chloroform-*d*): δ = 55.35, 149.08, 148.52, 144.67, 141.57,131.18, 130.74, 123.31, 121.21, 120.52, 113.98, 112.61, 111.32, 71.84, 70.57, 70.45, 70.37, 69.45, 58.95, 53.46, 51.15, 50.31, 46.60, 31.95, 31.44, 30.19, 29.77, 29.72, 29.68, 29.62, 29.39, 27.29, 22.71, 14.15. MS (MALDI-TOF): m/z calculated for $C_{128}H_{206}BF_2N_{19}O_{16}$, $[M]^+$ = 2316.0, found: 2316.4. Elemental analysis: calculated for $C_{128}H_{206}BF_2N_{19}O_{16}$: C 66.38%, H 8.97%, N 11.49%; found: C 66.65%, H 8.50%, N 10.85%. UV-Vis-NIR absorption (in $CHCl_3$): $\lambda_{max}(\varepsilon)$ = 805 (95 000), 648 (46 000), 430 (13 000), 380 (23 000 M^{-1} cm^{-1}); fluorescence (in $CHCl_3$): λ_{max} = 863 nm; fluorescence quantum yield (in $CHCl_3$): Φ_{fl} = 0.16.

Conflicts of interest

There are no conflicts to declare.

Data availability

The data supporting this article have been included as part of the supplementary information (SI). Supplementary information: ^{1}H NMR and ^{13}C NMR spectra, absorption and fluorescence spectra, and other results. See DOI: **https://doi.org/10.1039/d5ra06752a**.

Acknowledgements

The authors acknowledge the financial support of the National Natural Science Foundation of China (Grant No. 92056115).

Notes and references

1 (*a*) D. Ma, H. Bian, M. Gu, L. Wang, X. Chen and X. Peng, *Coord. Chem. Rev.*, 2024, **505**, 215677; (*b*) Y. Sun, P. Sun, Z. Li, L. Qu and W. Guo, *Chem. Soc. Rev.*, 2022, **51**, 7170–7205; (*c*) H. Li, Y. Kim, H. Jung, J. Y. Hyun and I. Shin, *Chem. Soc. Rev.*, 2022, **51**, 8957–9008.
2 L. Cheng, C. Wang, L. Feng, K. Yang and Z. Liu, *Chem. Rev.*, 2014, **114**, 10869–10939.
3 (*a*) J. H. Kim, T. Schembri, D. Bialas, M. Stolte and F. Würthner, *Adv. Mater.*, 2022, **34**, 2104678; (*b*) A. Barbieri, E. Bandini, F. Monti, V. K. Praveen and N. Armaroli, *Top. Curr. Chem.*, 2016, **374**, 47.
4 D. Wu, L. Chen, W. Lee, G. Ko, J. Yin and J. Yoon, *Coord. Chem. Rev.*, 2018, **354**, 74–97.
5 H. Chen, B. Dong, Y. Tang and W. Lin, *Acc. Chem. Res.*, 2017, **50**, 1410–1422.
6 (*a*) X. Fu, J. Wu, H. Xu, P. Wan, H. Fu and Q. Mei, *Anal. Chem.*, 2021, **93**, 15696–15702; (*b*) X. Liu, B. Yu, Y. Shen and H. Cong, *Coord. Chem. Rev.*, 2022, **468**, 214609; (*c*) Z. Zhang, A. Mei, W. Wang, K. Xu, M. Wang, P. Chen, J. Shao and X. Dong, *Coord. Chem. Rev.*, 2025, **545**, 217026.
7 L. Yuan, W. Lin, K. Zheng, L. He and W. Huang, *Chem. Soc. Rev.*, 2013, **42**, 622–661.
8 G. Deng, L. Sun, F. Zeng and S. Wu, *Anal. Methods*, 2024, **16**, 8316–8323.
9 P. Singh and P. Sharma, *J. Photochem. Photobiol., A*, 2021, **408**, 113096.
10 J. Gong, C. Liu, X. Jiao, S. He, L. Zhao and X. Zeng, *Org. Biomol. Chem.*, 2020, **18**, 5238–5244.
11 W. Shi, J. Liu and D. K. P. Ng, *Chem.–Asian J.*, 2012, **7**, 196–200.
12 (*a*) Y. Chen, S. Zheng, M. H. Kim, X. Chen and J. Yoon, *Curr. Opin. Chem. Biol.*, 2023, **75**, 102321; (*b*) X. Qian, H. Yu, W. Zhu, X. Yao, W. Liu, S. Yang, F. Zhou and Y. Liu, *Dyes Pigm.*, 2021, **188**, 109218.
13 Y. Ge and D. F. O'Shea, *Chem. Soc. Rev.*, 2016, **45**, 3846–3864.
14 A. Karatay, M. C. Miser, X. Cui, B. Küçüköz, H. Yılmaz, G. Sevinç, E. Akhüseyin, X. Wu, M. Hayvali, H. G. Yaglioglu, J. Zhao and A. Elmali, *Dyes Pigm.*, 2015, **122**, 286–294.
15 (*a*) J. Su, X. Zhang, Z. Dong, H. Pan, F. Zhang, X. Li, S. Wang and Z. Chen, *ACS Appl. Mater. Interfaces*, 2024, **16**, 51241–51252; (*b*) J. Zuo, H. Pan, Y. Zhang, Y. Chen, H. Wang,

X.-K. Ren and Z. Chen, *Dyes Pigm.*, 2020, **183**, 108714; (*c*) B. Lei, H. Pan, Y. Zhang, X. Ren and Z. Chen, *Org. Biomol. Chem.*, 2021, **19**, 6108–6114.

16 J. Wang, C. Yu, E. Hao and L. Jiao, *Coord. Chem. Rev.*, 2022, **470**, 214709.

17 J. Killoran, L. Allen, J. F. Gallagher, W. M. Gallagher and D. F. O'Shea, *Chem. Commun.*, 2002, 1862–1863.

18 J. Su, L. Zhu, Z. Dong, M. Liu, F. Zhang, X. Li, S. Wang and Z. Chen, *Org. Chem. Front.*, 2024, **11**, 7044–7052.

19 L. Bai, P. Sun, Y. Liu, H. Zhang, W. Hu, W. Zhang, Z. Liu, Q. Fan, L. Li and W. Huang, *Chem. Commun.*, 2019, **55**, 10920–10923.

20 (*a*) Y. Wu, C. Cheng, L. Jiao, C. Yu, S. Wang, Y. Wei, X. Mu and E. Hao, *Org. Lett.*, 2014, **16**, 748–751; (*b*) W. Sheng, Z. Wang, G. Wu, L. Guo, X. Guo, E. Hao and L. Jiao, *Org. Lett.*, 2025, **27**, 5977–5982; (*c*) X. Guo, W. Sheng, H. Pan, L. Guo, H. Zuo, Z. Wu, S. Ling, X. Jiang, Z. Chen, L. Jiao and E. Hao, *Angew. Chem., Int. Ed.*, 2024, **63**, e202319875.

21 Ö. Sonkaya, C. Soylukan, M. Pamuk Algi and F. Algi, *Curr. Org. Synth.*, 2023, **20**, 20–60.

22 (*a*) Y. Tachapermpon, S. Thavornpradit, A. Charoenpanich, J. Sirirak, K. Burgess and N. Wanichacheva, *Dalton Trans.*, 2017, **46**, 16251–16256; (*b*) P. Praikaew, T. Roongcharoen, A. Charoenpanich, N. Kungwan and N. Wanichacheva, *J. Photochem. Photobiol., A*, 2020, **400**, 112641; (*c*) Y. C. Pino, J. A. Aguilera, V. García-González, M. Alatorre-Meda, E. Rodríguez-Velázquez, K. A. Espinoza, H. Frayde-Gómez and I. A. Rivero, *ACS Omega*, 2022, **7**, 42752–42762; (*d*) H. Liu, J. Mack, Q. Guo, H. Lu, N. Kobayashi and Z. Shen, *Chem. Commun.*, 2011, **47**, 12092.

23 (*a*) C. Liu, W. Ding, Y. Liu, H. Zhao and X. Cheng, *New J. Chem.*, 2020, **44**, 102–109; (*b*) L. Zhang, L. Zou, J. Guo and A. Ren, *New J. Chem.*, 2016, **40**, 4899–4910; (*c*) N. Adarsh, M. Shanmugasundaram and D. Ramaiah, *Anal. Chem.*, 2013, **85**, 10008–10012.

24 (*a*) W. Mao, M. Zhu, C. Yan, Y. Ma, Z. Guo and W. Zhu, *ACS Appl. Bio Mater.*, 2020, **3**, 45–52; (*b*) N. Adarsh, M. S. Krishnan and D. Ramaiah, *Anal. Chem.*, 2014, **86**, 9335–9342.

25 G. R. You, G. J. Park, J. J. Lee and C. Kim, *Dalton Trans.*, 2015, **44**, 9120–9129.

26 H. Huang, S. Wong, K. Tian, J. Wang, M. Zhang, J. Tu, H. Pan, W. Ngeontae and X. Ren, *Talanta*, 2025, **292**, 127983.

27 B. Mahto, S. Chand, D. V. Singh, S. Patra and G. Chandra, *J. Mol. Struct.*, 2024, **1306**, 137839.

28 L. Loaeza, R. Corona-Sánchez, G. Castro, M. Romero-Ávila, R. Santillan, V. Maraval, R. Chauvin and N. Farfán, *Tetrahedron*, 2021, **83**, 131983.

29 C. E. A. De Melo, M. Domínguez, M. C. Rezende and V. G. Machado, *Dyes Pigm.*, 2021, **184**, 108757.

30 A. Kurutos and D. Citterio, *J. Mol. Struct.*, 2022, **1247**, 131381.

31 B. Wang, X. Zhang, X. Jia, Z. Li, Y. Ji, L. Yang and Y. Wei, *J. Am. Chem. Soc.*, 2004, **126**, 15180–15194.

32 M. Panneerselvam, A. Kathiravan, N. Johnee Britto, S. M. Krishnan, G. Velmurugan and M. Jaccob, *J. Mater. Sci.*, 2022, **57**, 10724–10735.

33 C. Reichardt, *Chem. Rev.*, 1994, **94**, 2319–2358.

34 G. Singh, N. George, R. Singh, G. Singh, Sushma, G. Kaur, H. Singh and J. Singh, *Appl. Organomet. Chem.*, 2023, **37**, e6897.

35 D. Y. Patil, N. B. Khadke, A. A. Patil and A. V. Borhade, *J. Anal. Chem.*, 2022, **77**, 18–25.

36 (*a*) S. Liu, Z. Shi, W. Xu, H. Yang, N. Xi, X. Liu, Q. Zhao and W. Huang, *Dyes Pigm.*, 2014, **103**, 145–153; (*b*) M. Pamuk and F. Algi, *Tetrahedron Lett.*, 2012, **53**, 7117–7120.

37 A. Balcerak and J. Kabatc, *J. Mol. Liq.*, 2020, **313**, 113489.

38 A. Amirjani, K. Salehi and S. K. Sadrnezhaad, *Spectrochim. Acta, Part A*, 2022, **268**, 120692.

39 Y. Liu, H. Yu, Y. Chen and Y. Zhao, *Chem.–Eur. J.*, 2006, **12**, 3858–3868.

40 H. Wu, M. Chen, Q. Xu, Y. Zhang, P. Liu, W. Li and S. Fan, *Chem. Commun.*, 2019, **55**, 15137–15140.

41 A. Hafuka, H. Satoh, K. Yamada, M. Takahashi and S. Okabe, *Materials*, 2018, **11**, 814–822.